

How important is organic aerosol hygroscopicity to aerosol indirect forcing?

Xiaohong Liu^{1,3} and Jian Wang²

¹ Atmospheric Science & Global Change Division, Pacific Northwest National Laboratory, 3200 Q Avenue, MSIN K9-24 Richland, WA 99352, USA

² Atmospheric Sciences Division, Brookhaven National Laboratory, Upton, NY 11973, USA

E-mail: Xiaohong.Liu@pnl.gov and jian@bnl.gov

Received 17 August 2010

Accepted for publication 10 November 2010

Published 7 December 2010

Online at stacks.iop.org/ERL/5/044010

Abstract

Organics are among the most abundant aerosol components in the atmosphere. However, there are still large uncertainties with emissions of primary organic aerosol (POA) and volatile organic compounds (VOCs) (precursor gases of secondary organic aerosol, SOA), formation of SOA, and chemical and physical properties (e.g., hygroscopicity) of POA and SOA. All these may have significant impacts on aerosol direct and indirect forcing estimated from global models. In this study a modal aerosol module (MAM) in the NCAR community atmospheric model (CAM) is used to examine sensitivities of aerosol indirect forcing to hygroscopicity (represented by a single parameter ' κ ') of POA and SOA. Our model simulation indicates that in the present-day (PD) condition changing the ' κ ' value of POA from 0 to 0.1 increases the number concentration of cloud condensational nuclei (CCN) at supersaturation $S = 0.1\%$ by 40–80% over the POA source regions, while changing the ' κ ' value of SOA by $\pm 50\%$ (from 0.14 to 0.07 and 0.21) changes the CCN concentration within 40%. There are disproportionately larger changes in CCN concentration in the pre-industrial (PI) condition. Due to the stronger impact of organics hygroscopicity on CCN and cloud droplet number concentration at PI condition, global annual mean anthropogenic aerosol indirect forcing (AIF) between PD and PI conditions reduces with the increase of the hygroscopicity of organics. Global annual mean AIF varies by 0.4 W m^{-2} in the sensitivity runs with the control run of -1.3 W m^{-2} , highlighting the need for improved understanding of organics hygroscopicity and its representation in global models.

Keywords: aerosol, organic, cloud, climate

1. Introduction

Atmospheric aerosols affect the global energy budget by scattering and absorbing sunlight (direct effects) and by changing the microphysics, lifetime, and coverage of clouds (indirect effects). An increase in aerosol concentration would lead to smaller cloud droplet size and higher cloud albedo, i.e., brighter clouds (Twomey 1977). This effect, which is known as the first indirect aerosol effect, tends to cool the global climate. The smaller cloud droplet size resulting from increased aerosol concentration also inhibits precipitation, leading to an increase

in cloud lifetime and coverage (second indirect aerosol effect, (Albrecht 1989)). Although it is widely accepted that the indirect effects can strongly influence the global climate, and potentially mask the warming effect due to anthropogenic CO_2 , the magnitudes of indirect aerosol effects are poorly understood. The Intergovernmental Panel on Climate Change (IPCC 2007) considers the indirect effects of aerosol the most uncertain components in forcing of climate change over the industrial period.

To understand the aerosol indirect effects requires knowledge of the cloud condensation nuclei (CCN) spectrum of aerosol particles, which is the number concentration of

³ Author to whom any correspondence should be addressed.

particles that can form cloud droplets as a function of water vapor supersaturation. The hygroscopicity of particles containing only soluble inorganic species typically found in atmospheric aerosols is well understood, and the CCN spectrum of the inorganic particles can be effectively predicted using Köhler theory (Köhler 1936). However, the composition of atmospheric particles is often very complex. Compared to the inorganic component, usually limited to a few species, the organic component of ambient aerosols may consist of hundreds or even thousands of species, which often contribute substantially to, or sometimes even dominate fine aerosol mass (Kanakidou *et al* 2005). A number of studies have shown that organic aerosols play an important role in both the direct and indirect aerosol forcing (e.g., Lohmann *et al* 2000, Chung and Seinfeld 2002, Kanakidou *et al* 2005, Goto *et al* 2008), which are highly uncertain (IPCC 2007). Direct radiative forcing of anthropogenic organic aerosol was estimated to be -0.06 to -0.23 W m^{-2} as compared to -0.16 to -0.58 W m^{-2} for anthropogenic sulfate from nine global models with the same prescribed emissions (Schulz *et al* 2006). At present there are large uncertainties in the emission inventories of primary organics aerosols and secondary aerosol formation in global models (Kanakidou *et al* 2005, Farina *et al* 2010). Furthermore, unlike typical inorganic aerosol species whose hygroscopicities are well understood, currently there are still large uncertainties in our understanding of the hygroscopicity of the organic species. Previous studies show atmospheric organics ranging from non-hygroscopic, such as primary organic aerosol emitted from fossil fuel combustion, to highly hygroscopic biomass burning organic aerosols (Carrico *et al* 2008, Petters *et al* 2009). Given the computational constraints, the large number of organic species often can only be represented by no more than a few classes in global models. This presents further challenges in simulating aerosol indirect forcing (AIF). In this study, a version of the NCAR Community Atmospheric Model (CAM) is used to examine the uncertainties in global simulated CCN concentration, cloud droplet number concentration (CDNC), and AIF arising from the uncertainty in our understanding of organic aerosol hygroscopicity. In the CAM, the activation of aerosol particles is represented using a parameterization (Abdul-Razzak and Ghan 2000) based on Köhler theory, which directly takes into consideration the effects of particle size, composition, and hygroscopicity of participating species (including organics) on particle activation. As far as we know, this is the first study examining the uncertainty in global averaged AIF due to the uncertainties in organic hygroscopicity. The implication on future study of the hygroscopicity of organic aerosol is also discussed.

2. Model

We use the NCAR Community Atmospheric Model (CAM) for all the simulations. This model version starts with CAM version 3 (Collins *et al* 2006) with several important changes added. The deep convection scheme closure has been modified following Neale *et al* (2008). The shallow convection scheme is based on Park and Bretherton (2009), and the moisture

boundary layer scheme is based on Bretherton and Park (2009). The radiation code has been updated to the rapid radiative transfer model for GCMs (RRTMG) as described by Iacono *et al* (2008). The liquid cloud macrophysics closure is described by Park *et al* (2010). This CAM version is designed to simulate fully interactive aerosol direct and indirect effects. For that, a two-moment stratiform cloud microphysics is included which predicts the mass and number mixing ratio of cloud water and cloud ice, and diagnoses the mass and number mixing ratio of precipitation (rain and snow) (Morrison and Gettelman 2008). The cloud ice microphysics was further modified to allow ice supersaturation and aerosol effect on ice clouds (Gettelman *et al* 2010).

The new modal aerosol module (MAM) is based on Easter *et al* (2004) but includes many updates for aerosol treatment and has a simplified three-mode version added for long-term climate simulations (Liu *et al* 2010). The benchmark version of MAM with seven aerosol modes (MAM-7) is used here. It includes Aitken, accumulation, primary carbon, fine dust and sea salt and coarse dust and sea salt modes. The predicted internally mixed aerosol species for each log-normal mode in MAM-7 are listed in table 1. In MAM, the interstitial aerosol particles that are suspended in air (either clear or cloudy air) and the aerosol particles in stratiform cloud droplets (referred to as cloud-borne aerosol particles) are both explicitly predicted, as in Easter *et al* (2004). The cloud-borne aerosol particles are not transported, which saves computer time but has little impact on their predicted values (Ghan and Easter 2006). Below we will provide more description on the treatment of organic aerosol and aerosol activation most relevant to this study. Further detailed description on aerosol processes and properties treated in MAM can be found in the CAM scientific document (Neale *et al* 2010).

In MAM, the organic species are grouped into two classes. The first class, named as primary organic aerosol (POA), includes primary organics emitted due to both fossil fuel and bio-fuel consumption (industry, energy, transportation, agriculture waste burning, waste treatment, domestic emission and shipping) and biomass burning (forest fire and grass fire) (Lamarque *et al* 2010). The second class, referred to as secondary organic aerosol (SOA), includes secondary organics formed from anthropogenic and biogenic precursors. Carbonaceous aerosols (POA and black carbon (BC)) are emitted in the primary carbon mode (see table 1) and age to the accumulation mode through condensation of sulfuric acid gas (H_2SO_4), ammonia (NH_3), and secondary organic aerosol gas (SOA (gas)) and coagulation with Aitken and accumulation mode. The simplest treatment of SOA, which is used in many global models, is to assume fixed mass yields for anthropogenic and biogenic volatile organic compounds (VOCs), then directly emit this mass as primary aerosol particles. MAM adds one additional step of complexity by simulating a single lumped gas-phase SOA (gas) species. Fixed mass yields with values of 5%, 5%, 15%, 4% and 25% are assumed for big alkanes, big alkenes, toluene, isoprene and monoterpenes, respectively of the five VOC categories in the MOZART-4 gas-phase chemical mechanism (Emmons *et al* 2010). References for these yields can be found in Neale *et al*

Table 1. Predicted species for interstitial and cloud-borne component of each aerosol mode in MAM-7. (Note: mmr—mass mixing ratio.)

Aitken mode	Accumulation mode	Fine soil dust	Fine sea salt
Number mixing ratio	Number mixing ratio	Number mixing ratio	Number mixing ratio
Sulfate mmr	Sulfate mmr	Soil dust mmr	Sea salt mmr
Ammonium mmr	Ammonium mmr	Sulfate mmr	Sulfate mmr
Sea salt mmr	Sea salt mmr	Ammonium mmr	Ammonium mmr
Secondary organic mmr	Secondary organic mmr		
	Aged primary organic mmr		
	Aged BC mmr		
	Primary carbon mode	Coarse soil dust	Coarse sea salt
	Number mixing ratio	Number mixing ratio	Number mixing ratio
	Primary organic mmr	Soil dust mmr	Sea salt mmr
	BC mmr	Sulfate mmr	Sulfate mmr
		Ammonium mmr	Ammonium mmr

Table 2. Organics hygroscopicity from previous measurements.

Organics class	Range of κ	References
Biogenic SOA	0.06–0.23	Prenni <i>et al</i> (2007), King <i>et al</i> (2007), Duplissy <i>et al</i> (2008), Engelhart <i>et al</i> (2008), Gunthe <i>et al</i> (2009), Juranyi <i>et al</i> (2009), King <i>et al</i> (2009), King <i>et al</i> (2010)
Anthropogenic SOA	0.06–0.14	Prenni <i>et al</i> (2007)
Biomass burning organic aerosol	0.06–0.30	Vestin <i>et al</i> 2007, Asa-Awuku <i>et al</i> (2008), Carrico <i>et al</i> (2008), Gunthe <i>et al</i> (2009), Petters <i>et al</i> (2009)

Table 3. Simulations performed in this study.

Case name	Description
CTL	Standard CAM, $\kappa = 0.0$ (POA), $\kappa = 0.14$ (SOA)
POA-hiK	$\kappa = 0.1$ (POA), $\kappa = 0.14$ (SOA)
SOA-loK	$\kappa = 0.0$ (POA), $\kappa = 0.07$ (SOA)
SOA-hiK	$\kappa = 0.0$ (POA), $\kappa = 0.21$ (SOA)

(2010). The total yielded mass is emitted as the SOA (gas) species. MAM then calculates condensation/evaporation of the SOA (gas) to/from aerosol modes (Aitken and accumulation mode).

Organic aerosol can affect stratiform cloud microphysics through participating in activation. The hygroscopicity of each component (including POA and SOA) is prescribed in MAM, and the volume mean hygroscopicity for each aerosol mode containing different components is calculated (Ghan and Zaveri 2007). Aerosol activation is parameterized in terms of sub-grid cloud scale vertical velocity, size distribution and volume mean hygroscopicity of all of the aerosol modes (Abdul-Razzak and Ghan 2000). The updraft velocity is approximated by the square root of the turbulence kinetic energy, and with a minimum value of 0.2 m s^{-1} . A peak supersaturation is diagnosed in the Abdul-Razzak and Ghan (2000) parameterization which determines the critical size of aerosols in each mode activated to become cloud droplets. We note that currently the effects of organic aerosol on convective and ice cloud microphysics are not included in the CAM.

The hygroscopicities of POA and SOA are parameterized using the B value (Hudson and Da 1996), which is practically equivalent to the single parameter κ proposed by Petters and Kreidenweis (2007). In this study, the single parameter κ is used, as many recent measurements of organic hygroscopicity are reported in κ . Table 2 lists the κ values of secondary organics aerosols and biomass burning organic aerosol

reported from previous studies, including field measurements and environmental chamber studies. While fossil fuel primary organics are generally considered as non-hygroscopic (i.e. $\kappa = 0$), previous studies show that biomass burning organic aerosol and secondary organic aerosols are generally hygroscopic with κ ranged from 0.06 to 0.30. In addition, previous field studies suggest that the hygroscopicity of SOA increases from ~ 0 to 0.2 during its ageing in the atmosphere (Jimenez *et al* 2009). To test the effects of hygroscopicity of organic aerosol on CCN and indirect forcing, we run the CAM by varying κ values for POA and SOA as listed in table 3, for pairs of present-day (PD) and pre-industrial (PI) simulations. In one of the cases, the κ value of the POA is increased from 0 in the control case to 0.1 to account for the hygroscopicity of biomass burning organics. The κ value of SOA is also varied from 0.14 in the control case by $\pm 50\%$ to represent the range of κ values of SOA reported from earlier measurements.

3. Results

The CAM model is run for 5 years with 3-month spin-up with fixed sea surface temperatures. Anthropogenic (defined here as originating from industrial, domestic and agriculture activity sectors) emissions are from the Lamarque *et al* (2010) IPCC AR5 emission data set for the year 2000 (PD simulation) and the year 1850 (PI simulation). The IPCC AR5 emission data set does not provide injection heights. We used the injection heights from the AEROCOM emission protocol (Dentener *et al* 2006) to distribute the IPCC AR5 emissions from energy and industrial sectors at 100–300 m above the surface, and emissions from forest fire and grass fire at 0–6 km. We used the size distributions of primary emitted particles (sulfate, POA and BC) from the AEROCOM (Dentener *et al* 2006) to convert IPCC AR5 mass emission fluxes to number emission fluxes.

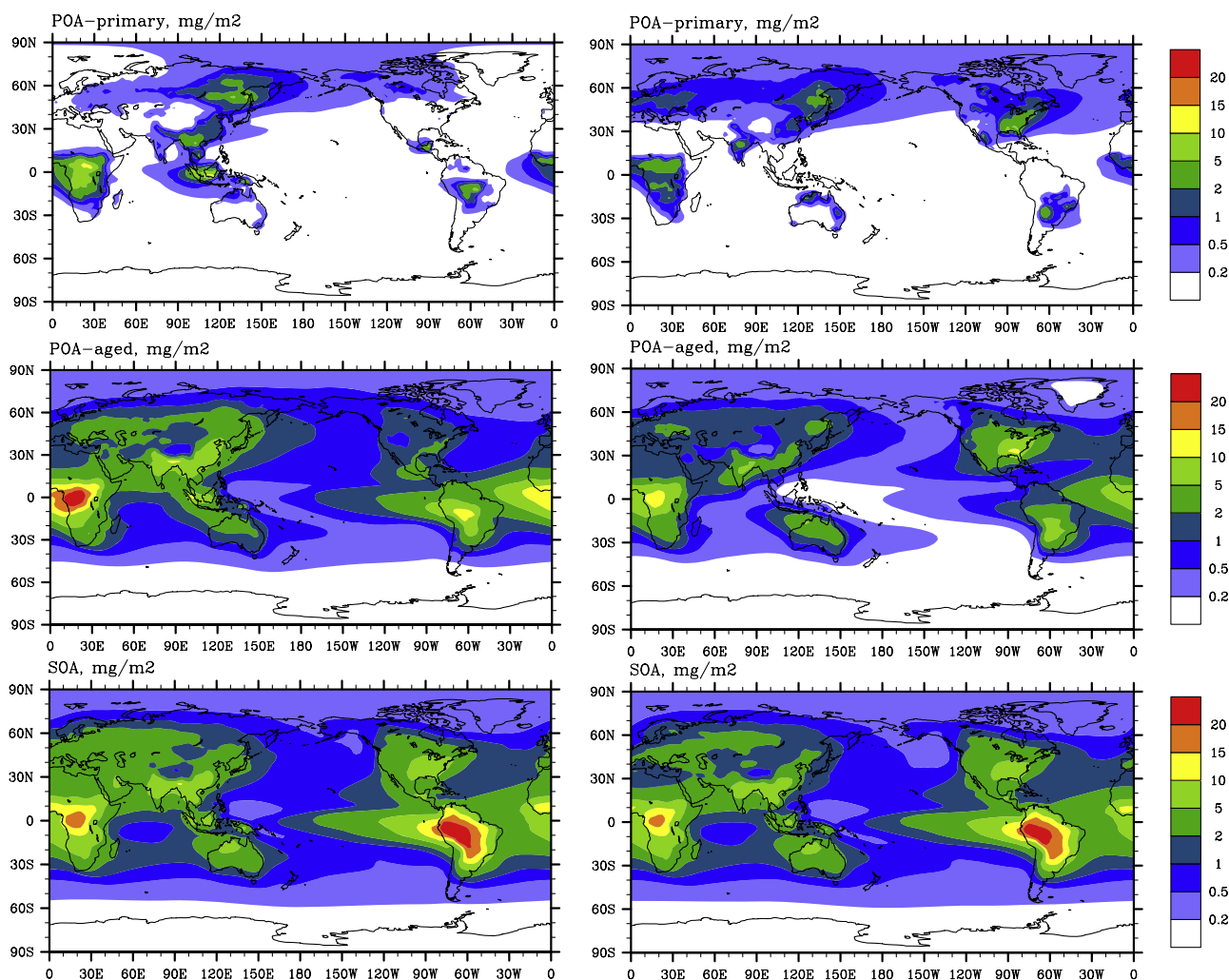


Figure 1. Annual means of column burden concentrations (mg m^{-2}) of POA in primary carbon mode (upper panel) and aged POA in the accumulation mode (middle panel), and SOA (lower panel) in the CTL run at PD (left) and at PI (right).

For POA/BC, the emitted number mean radius is $0.04 \mu\text{m}$ with a standard deviation of 1.8. The IPCC AR5 emission data set does not provide emissions for natural aerosols and precursor gases (e.g., volcanic sulfur, dimethyl sulfide (DMS)), for which we have followed the AEROCOM protocols (Dentener *et al* 2006).

Figure 1 shows annual means of column burden concentrations of POA in primary carbon mode and POA aged to the accumulation mode, and SOA from the PD and PI control run. Clearly POA from primary emissions (e.g., fossil fuel, bio-fuel, and biomass burning) is aged to the accumulation mode quickly, e.g., at PD in the industrial regions where sulfate concentrations are high. This result is in general agreement with observations that carbonaceous aerosol particles are internally mixed with sulfate and other components except near the source regions (e.g., Posfai *et al* 2003, Clarke *et al* 2004, Moffet and Prather 2009, Wang *et al* 2010). SOA column concentrations have spatial distributions similar to aged POA, and both have high concentrations in the industrial regions and in the biomass burning regions (central Africa and South America), although their seasonal variations are different (results not shown). The global spatial

distributions of POA (in primary and accumulation modes) and SOA column concentrations are similar between PD and PI. However, there are several noticeable differences: aged POA concentration in the accumulation mode at PD in South and East Asia, Indonesia and in central Africa and South America is much higher than that at PI due to emission differences, while POA concentration in Eastern US is higher at PI due to more emissions from forest and grass fire and domestic heating there at PI (Lamarque *et al* 2010).

The global budgets for organic aerosol (POA in primary and accumulation mode, and SOA) are given in table 4. POA in the primary mode ages to the accumulation mode with a lifetime of 1.2–1.5 days. There is a longer lifetime for POA in the primary mode at PI than that at PD due to significantly less sulfate available for ageing at PI (see figure 2 below). The global burden of aged POA in the accumulation mode is 4–6 times higher than that in the primary mode. Fossil and bio-fuel POA emission at PI is 36% of that at PD, however, that from biomass burning at PI is 78% of that at PD. Total POA at PI is 63% of that at PD mainly due to the lower fossil fuel and bio-fuel POA emission sources at PI. SOA (g) formation is dominated from the oxidation of biogenic VOCs (isoprene and

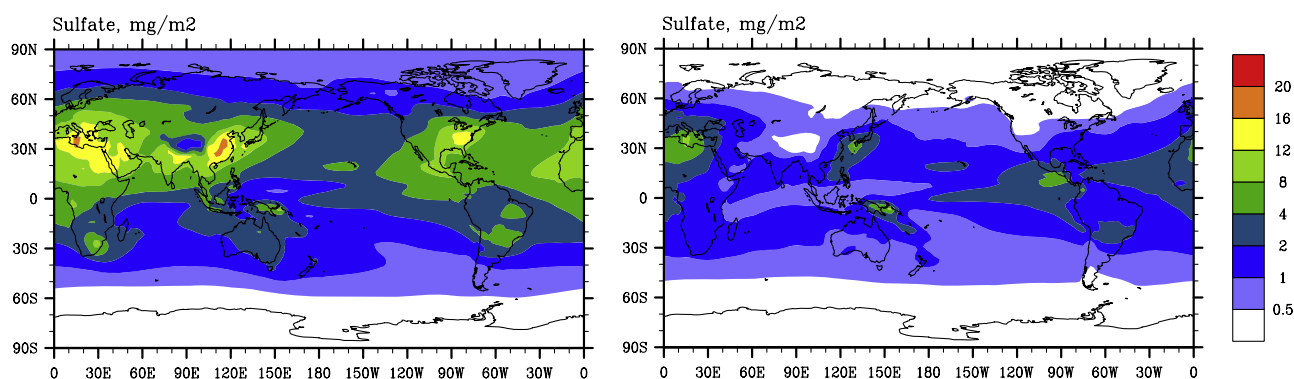


Figure 2. Annual means of column burden concentration (mg m^{-2}) of sulfate in the control (CTL) run at PD (left) and at PI (right).

Table 4. Global budgets for organic aerosol from the control (CTL) run at PD and PI. (Note: units are sources and sinks, Tg yr^{-1} ; burden, Tg ; lifetime, days.)

	PD	PI
POA (primary mode)		
Sources		
Fossil and bio-fuel emission	16.8	6.0
Biomass burning emission	32.5	25.2
Sinks		
Dry deposition	2.9	2.2
Wet deposition	0.005	0.003
Aged to accumulation mode	46.4	29.0
Burden	0.16	0.13
Lifetime	1.2	1.5
POA (accumulation mode)		
Sources		
Aged from primary mode	46.4	29.0
Sinks		
Dry deposition	7.2	4.8
Wet deposition	39.3	24.3
Burden	0.95	0.56
Lifetime	7.5	7.0
SOA		
Sources		
Condensation of SOA (g)	68.6	61.5
Sinks		
Dry deposition	9.8	8.1
Wet deposition	58.7	53.3
Burden	1.26	1.13
Lifetime	6.7	6.8

monoterpenes) in this study. Therefore we see only a slight reduction of SOA burden (by 10%) at PI compared to PD. The global SOA production (68.6 Tg yr^{-1} at PD) in this study is higher than values from the earlier studies of 11.2 Tg yr^{-1} by Chung and Seinfeld (2002), 19.1 Tg yr^{-1} by Dentener *et al* (2006), and $10\text{--}60 \text{ Tg yr}^{-1}$ by Kanakidou *et al* (2005), and within the range of 28.9 to 75.1 Tg yr^{-1} from a more recent study by Farina *et al* (2010). The SOA burden of 1.26 Tg at PD in this study is higher than 0.19 Tg from Chung and Seinfeld (2002), but within the range of $0.54\text{--}2.4 \text{ Tg}$ from Farina *et al* (2010).

Figure 2 shows annual means of column burden concentrations of sulfate from the PD and PI control run. Sulfate column concentrations have maximum values in the

industrial regions (Asia, North America and Europe) at PD, and are significantly lower at PI. At PD, sulfate column concentrations are slightly higher than those of aged POA and SOA in the industrial regions, whereas at PI, sulfate column concentrations are much lower (e.g., in Asia and North America). The global annual burden of sulfate is 0.61 Tg S at PD (within the range of $0.53\text{--}1.07 \text{ Tg S}$ from literature collected in Liu *et al* (2005)) and 0.21 Tg S at PI.

Figure 3 shows percentage changes of cloud condensational nuclei (CCN) concentration at supersaturation of 0.1% at 859 hPa between the sensitivity simulations listed in table 3 and the control (CTL) simulation at PD and at PI. Here CCN concentration diagnosed at a given supersaturation (0.1%) is used to show the impact of aerosols on cloud droplet number concentration, as the spatial distribution of changes in model predicted cloud droplet number concentration between different simulations is quite noisy due to cloud dynamical and thermodynamical feedbacks. CCN concentration at a given supersaturation is determined by a parameterization based on Köhler theory (Ghan and Zaveri 2007). The parameterization takes into consideration both the aerosol size distribution (represented by each mode) and volume weighted κ value from aerosol components (including organics) in each mode. For a given supersaturation and a fixed size distribution, an increase in κ value leads to lower critical dry size for activation, and higher CCN concentration as predicted from Köhler theory. From figure 3 at PD, an increase in κ value for POA from 0 to 0.1 increases CCN concentrations at 859 hPa by $20\text{--}80\%$ over the POA source regions (see figure 1). There are also some reductions by $10\text{--}20\%$ in the Arctic in the downwind of Siberia and Northern Canada due to more scavenging of POA in primary carbon mode when activated into cloud droplets at a higher κ value. A reduction of κ value for SOA from 0.14 to 0.07 at PD leads to reductions of CCN concentrations almost everywhere over the continents. The rainforest source regions (e.g., central Africa and South America) have reductions of $20\text{--}40\%$, as well as in the boreal and Arctic regions. CCN number reductions in the industrial regions are small (within 10%) because there is sufficient sulfate there to compensate aerosol hygroscopicity reduction due to SOA. An increase of κ value for SOA from 0.14 to 0.21 at PD has a similar impact on CCN concentrations to increasing the κ value for POA, although the magnitude is smaller (within 40% increase).

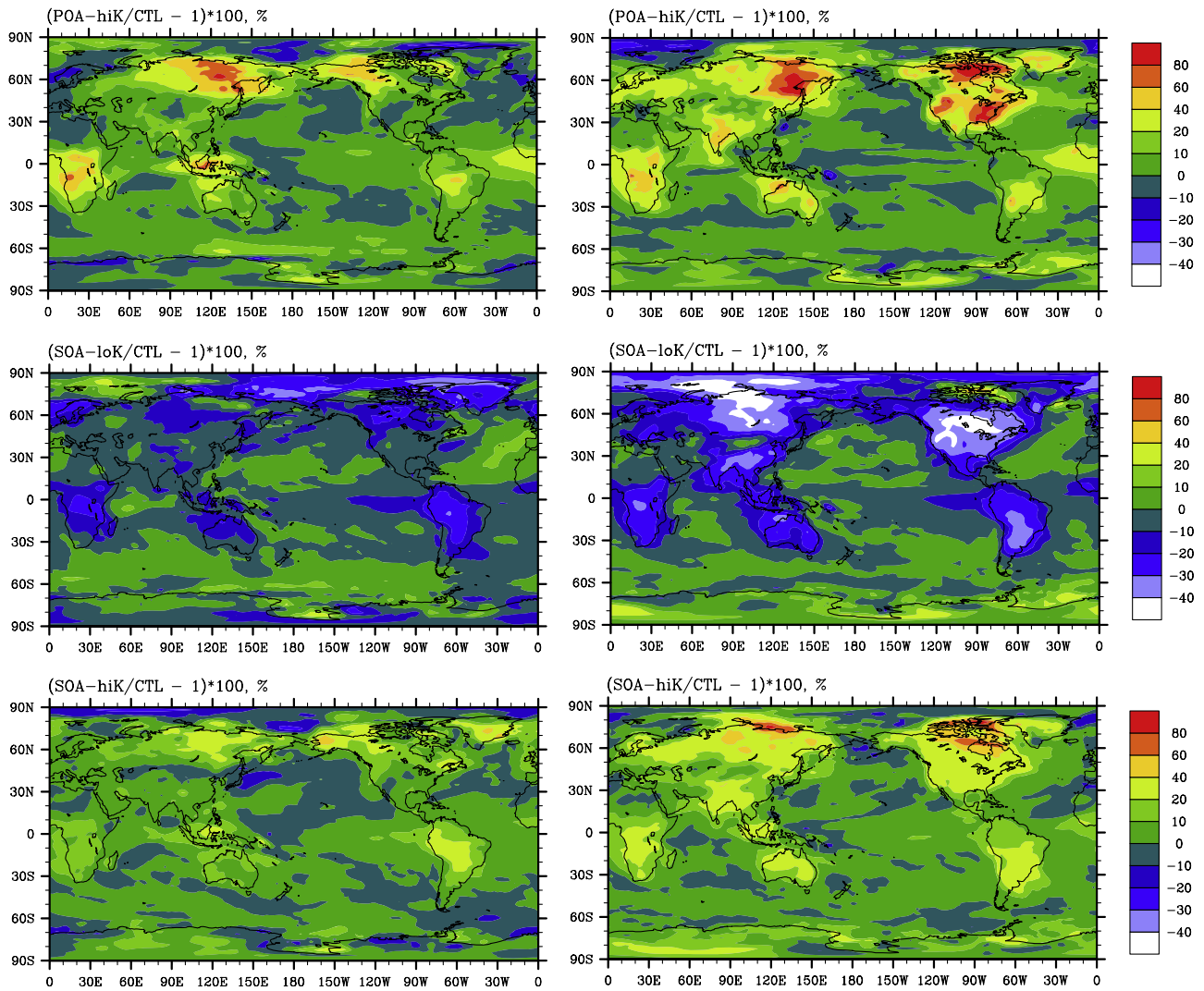


Figure 3. Percentage changes of cloud condensational nuclei (CCN) concentration at supersaturation of 0.1% at 859 hPa between the sensitivity simulations (POA-hiK, SOA-loK, and SOA-hiK) and the control simulation (CTL) at PD (left) and at PI (right).

Figure 3 also shows the changes of CCN concentration at PI. In general the same changes in κ value have much larger effects on CCN concentration at PI compared to those at PD. An increase in POA κ value increases CCN concentration significantly in the industrial source regions (North America, Asia, and Europe) at PI, which is, however, much less pronounced at PD. As indicated in figure 2, POA is aged to the accumulation mode and internally mixed with sulfate and other components quickly, especially in the industrial regions (e.g., Asia) and at PD when sulfate concentrations are higher than those at PI. As a result, the variation in CCN concentration resulting from varying POA κ value is generally small in the industrial regions at PD. This is in agreement with earlier studies that show for internally mixed particles, their hygroscopicity is dominated by inorganics such as sulfate and ammonium, and the influence of organic hygroscopicity on calculated CCN concentration is often minor there (Chang *et al* 2007, Prenni *et al* 2007, Wang *et al* 2008). In contrast, at PI when sulfate loading is substantially less, organics represent a larger fraction of particle volume. As a result, an increase in κ

value of POA leads to relatively larger increase in calculated CCN concentration. This disproportional change in CCN concentration can also be found with a reduction or increase in SOA κ value.

Table 5 gives the global annual mean vertically integrated (column) CCN concentration at supersaturation of 0.1% and column cloud droplet number concentration (CDNUMC) for all four runs listed in table 3 at PD and PI. Clearly there are larger changes in both CCN and CDNUMC concentrations at PI compared to PD as κ values vary. We note that global mean CCN column concentration at supersaturation of 0.1% is substantially higher than CDNUMC. This is because CCN concentration at supersaturation of 0.1% is calculated for the three-dimensional aerosol fields predicted in the model, whereas model predicted cloud droplet number concentration is limited to the cloudy regions where cloud droplets exist.

Figure 4 shows annual zonal mean changes of CDNUMC, shortwave cloud forcing (SWCF), liquid water path (LWP) and low-level cloud cover (CLDLow) between PD and PI for the four simulations listed in table 3. We note that cloud response

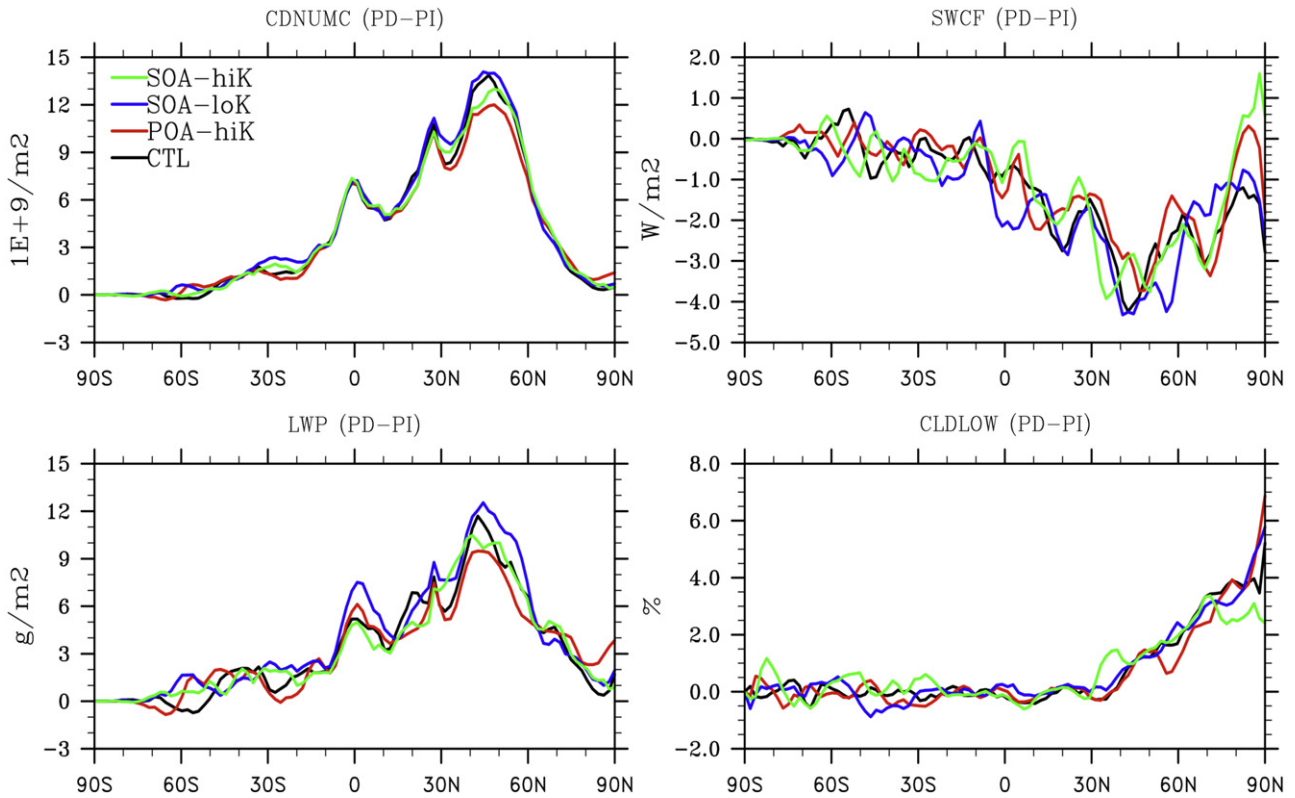


Figure 4. Annual zonal mean changes of column cloud droplet number concentration (CDNUMC), shortwave cloud forcing (SWCF), liquid water path (LWP) and low-level cloud cover (CLDLow) between PD and PI for the four simulations.

Table 5. Global annual mean vertically integrated (column) cloud condensational nuclei (CCN) concentration ($\times 10^{10} m^{-2}$) at supersaturation of 0.1% and cloud droplet number concentration (CDNUMC, $\times 10^9 m^{-2}$) for all four runs at PD and PI.

Case name	CTL	POA-hiK	SOA-loK	SOA-hiK
Column CCN ^a				
PD	25.6	27.6(+7.8%)	23.7(-7.4%)	27.3(+6.6%)
PI	14.9	16.7(+12.1%)	12.9(-13.4%)	16.6(+11.4%)
CDNUMC ^a				
PD	14.8	15.0(+1.3%)	14.3(-3.4%)	15.1(+2.1%)
PI	9.9	10.4(+5.1%)	9.1(-8.1%)	10.3(+4.0%)

^a The values in parentheses are for the percentage changes of column CCN concentration and CDNUMC between the sensitivity runs (POA-hiK, SOA-loK, and SOA-hiK) and the control run (CTL) for both PD and PI.

to anthropogenic aerosol perturbations may be noisy especially in the southern hemisphere (SH) due to natural variability and feedbacks of cloud dynamics and thermodynamics. However, we can clearly see that the SWCF increases (more negative) by as much as $4 W m^{-2}$ in the northern hemisphere (NH) mid-latitudes due to more numerous and smaller cloud droplets in PD compared to PI. An increase of LWP by $10 g m^{-2}$ is found in the NH mid-latitudes due to the second aerosol indirect effect to slow down the autoconversion of cloud water to rain. In addition, CLDLow increases by 2–3% in the NH high latitudes due to Arctic amplification from snow-ice feedbacks. Comparing with the control run, a higher

κ value of POA (POA-hiK run) reduces the difference of CDNUMC between PD and PI (e.g., in 20–60°N by 20–30%) due to more CCN and cloud droplet number increase at PI. Correspondingly, SWCF and LWP changes between PD and PI are reduced. A lower κ value of SOA (SOA-loK run) enhances the difference in CDNUMC between PD and PI (e.g., in 20–60°N and in 20–30°S) due to more CCN and cloud droplet number reduction at PI, and thus changes in SWCF and LWP between PD and PI are increased (e.g., in 20–60°N and in the tropics). Similarly, a higher κ value of SOA (SOA-hiK run) reduces the differences of CDNUMC, SWCF and LWP between PD and PI. Changes in CLDLow between PD and PI are not much different between different runs except in the Arctic regions for the SOA-hiK run. However, in the high latitudes where surface areas are relatively small the change signals may be just due to natural noise.

The global, NH and SH annual mean changes between PD and PI of SWCF, LWP, CLDLow and CDNUMC for different runs are listed in table 6. AIF is defined here as SWCF change between PD and PI as LWCF change is much smaller ($0.1 W m^{-2}$). We can see that AIF has the largest difference between POA-hiK and SOA-loK runs (by $0.4 W m^{-2}$ on the global mean) along with largest change in ΔLWP between these two runs (by $1 g m^{-2}$ on the global mean), in consistency with the smallest increase in POA-hiK ($4.6 \times 10^9 m^{-2}$ on the global mean) and the largest increase of CDNUMC between PD and PI in SOA-loK ($5.2 \times 10^9 m^{-2}$ on the global mean). Changes between PD and PI ($\Delta SWCF$, ΔLWP , $\Delta CLDLow$ and $\Delta CDNUMC$) for all four runs occur mainly in the NH due to more anthropogenic emissions. Differences of $\Delta SWCF$,

Table 6. Global, northern hemisphere (NH) and southern hemisphere (SH) annual mean changes (Δ) of shortwave cloud forcing (SWCF, $W m^{-2}$), liquid water path (LWP, $g m^{-2}$), low-level cloud cover (CLDLow, %), and column droplet number concentration (CDNUMC, $\times 10^9 m^{-2}$) between PD and PI (PD-PI) for all runs.

Case name		CTL ^a	POA-hiK	SOA-loK	SOA-hiK
Δ SWCF	Global	-1.3	-1.1	-1.5	-1.2
	NH	-2.2	-1.9	-2.5	-2.0
	SH	-0.3	-0.3	-0.4	-0.4
Δ LWP	Global	3.9	3.6	4.6	3.8
	NH	6.3	5.7	7.2	6.0
	SH	1.5	1.5	2.0	1.6
Δ CLDLow	Global	0.3	0.2	0.3	0.3
	NH	0.6	0.5	0.7	0.6
	SH	0.0	-0.1	-0.1	0.0
Δ CDNUMC	Global	4.9	4.6	5.2	4.8
	NH	8.0	7.4	8.3	7.7
	SH	1.8	1.8	2.1	1.9

^a Global annual mean SWCF, LWP, CLDLow, and CDNUMC of the control run at PD are $-47.1 W m^{-2}$, $45.6 g m^{-2}$, 37.1% , and $14.8 \times 10^9 m^{-2}$, respectively.

Δ LWP and Δ CDNUMC between different runs with varying κ value are also larger in the NH than those in the SH.

4. Discussion

There are large uncertainties in both the sources and the properties of organic aerosol. In this study we focus on the sensitivity of modeled AIF to the hygroscopicity of organic aerosol, which influences the ability of particles to activate into cloud droplets. The simulation results show that the uncertainty in organics aerosol hygroscopicity, based on current understanding and our model formulation, may lead to an uncertainty of about $0.4 W m^{-2}$ (-1.1 to $-1.5 W m^{-2}$) in AIF, which represents 1/3 of AIF simulated in the control case ($-1.3 W m^{-2}$). This uncertainty is comparable to or even larger than those due to autoconversion parameterization and tuning parameters related to entrainment, drizzle and snow formation (Liu *et al* 2008, Lohmann and Ferrachat 2010).

As expected, AIF is most significant in the NH, where anthropogenic influence is the strongest. It is worth noting that whereas a variation in organic hygroscopicity may lead to substantial changes in CCN concentration and CDNC in pristine environments (e.g. tropical forest), such changes have no impact on AIF there in the absence of anthropogenic aerosols, as AIF represents the difference between PD and PI. However, our results also highlight the important impact on AIF from organic aerosol, especially in the polluted NH mid-latitudes. Whereas an increase of POA κ value from 0 (control run) to 0.1 (POA-hiK run) leads to expected increases in CCN concentration at PD, the increase of CDNC from PI to PD is reduced, and the AIF decreases from -1.3 to $-1.1 W m^{-2}$ at the higher κ value of POA. This is due to disproportional impacts of POA κ value on CCN concentration at PD and PI in areas with substantial anthropogenic influence at PD (e.g., NH mid-latitudes). This feature is highlighted in figure 3, which shows larger increases in CCN concentration

due to the increase of POA κ value at PI compared to those at PD, especially in the industrial regions. This disproportional change in CCN concentration reduces the magnitude of the perturbation due to anthropogenic influences as we can see that the CDNUMC change from PI to PD in figure 4 and table 6 is reduced. Similarly, a decrease in κ value of SOA (SOA-loK run) leads to more pronounced decrease in CCN concentration at PI compared to PD, and therefore increases CDNUMC and LWP differences between PD and PI and thus AIF. Given the large contribution of biogenic SOA and biomass burning POA to the budget of organic aerosol, further constraint of their hygroscopicity in global models will help to reduce the uncertainty in simulated AIF.

An implicit assumption in the simulations is that for both organics classes, their hygroscopicities do not change from PI to PD. Anthropogenic emissions can strongly influence ozone and nitrogen oxide (NO_x) concentrations, which have been shown to impact the formation of secondary organic aerosols (Kanakidou *et al* 2005, Presto *et al* 2005, Dommen *et al* 2006, Kroll *et al* 2006, Ng *et al* 2007, Carlton *et al* 2009). Studies also suggest the VOC to NO_x ratio may influence the composition of SOA formed from biogenic VOC and therefore potentially its κ value. A recent study finds little variation in the κ value of SOA formed from isoprene photo-oxidation at different VOC to NO_x ratios (King *et al* 2010). However, there have been essentially no studies on the impact of NO_x on the κ value of SOA formed from other biogenic precursors. While the SOA κ value may have relatively small impact on calculated CCN concentration for PD due to the internal mixing with high-hygroscopic inorganic species, this change of SOA κ value from PI to PD as a result of anthropogenic influence may lead to additional uncertainty in simulated AIF.

The biomass burning organics and biogenic secondary organics dominate the budgets of POA and SOA, especially for PI. Currently, the experimentally determined κ values of SOA and biomass burning POA show a range of 0.06 to ~ 0.3 . Given the importance of understanding the CCN concentration at PI, the κ values of SOA and biomass burning POA need to be better understood and represented in models to reduce the uncertainties in AIF. As fossil fuel POA and biomass burning POA have quite different hygroscopicities, separating the two types of POA in future model development would improve the simulation of AIF. Furthermore, ageing processes in the atmosphere can also lead to the increase of hygroscopicity of POA and SOA. Field studies suggest that the κ value of SOA increases from 0 to ~ 0.2 during ageing in the atmosphere (Jimenez *et al* 2009), a range that is even greater than that simulated in the current study. The representation of this change of κ due to atmospheric ageing is also an important step for improving the simulation of AIF. Besides organics hygroscopicity, large uncertainties also exist on the SOA formation simulated in global models. The impact of organics formation on AIF will be examined in future studies.

Acknowledgments

X Liu was funded by the US Department of Energy, Office of Science, Atmospheric System Research (ASR) program and

Scientific Discovery through Advanced Computing (SciDAC) program. J Wang is funded by the US Department of Energy (DOE), Office of Science, ASR program. The Pacific Northwest National Laboratory is operated for DOE by Battelle Memorial Institute under contract DE-AC06-76RLO1830. The Brookhaven National Laboratory is operated for DOE by Brookhaven Science Associates, LLC under contract DE-AC02-98CH10886.

References

- Abdul-Razzak H and Ghan S J 2000 A parameterization of aerosol activation 2. Multiple aerosol types *J. Geophys. Res.* **105** 6837–44
- Albrecht B A 1989 Aerosols, cloud microphysics, and fractional cloudiness *Science* **245** 1227–30
- Asa-Awuku A, Sullivan A P, Hennigan C J, Weber R J and Nenes A 2008 Investigation of molar volume and surfactant characteristics of water-soluble organic compounds in biomass burning aerosol *Atmos. Chem. Phys.* **8** 799–812
- Bretherton C S and Park S 2009 A new moist turbulence parameterization in the community atmosphere model *J. Clim.* **22** 3422–48
- Carlton A G, Wiedinmyer C and Kroll J H 2009 A review of secondary organic aerosol (SOA) formation from isoprene *Atmos. Chem. Phys.* **9** 4987–5005
- Carrico C M, Petters M D, Kreidenweis S M, Collett J L, Engling G and Malm W C 2008 Aerosol hygroscopicity and cloud droplet activation of extracts of filters from biomass burning experiments *J. Geophys. Res.* **113** D08206
- Chang R Y W, Liu P S K, Leitch W R and Abbatt J P D 2007 Comparison between measured and predicted CCN concentrations at Egbert, Ontario: focus on the organic aerosol fraction at a semi-rural site *Atmos. Environ.* **41** 8172–82
- Chung S H and Seinfeld J H 2002 Global distribution and climate forcing of carbonaceous aerosols *J. Geophys. Res.* **107** 4407
- Clarke A D *et al* 2004 Size distributions and mixtures of dust and black carbon aerosol in Asian outflow: physicochemistry and optical properties *J. Geophys. Res.* **109** D15S09
- Collins W D *et al* 2006 The formulation and atmospheric simulation of the community atmosphere model: CAM3 *J. Clim.* **19** 2122–61
- Dentener F *et al* 2006 Emissions of primary aerosol and precursor gases in the years 2000 and 1750 prescribed data-sets for AeroCom *Atmos. Chem. Phys.* **6** 4321–44
- Dommen J, Metzger A, Duplissy J, Kalberer M, Alfarra M R, Gascho A, Weingartner E, Prevot A S H, Verheggen B and Baltensperger U 2006 Laboratory observation of oligomers in the aerosol from isoprene/NO_x photooxidation *Geophys. Res. Lett.* **33** L13805
- Duplissy J *et al* 2008 Cloud forming potential of secondary organic aerosol under near atmospheric conditions *Geophys. Res. Lett.* **35** L03818
- Easter R C *et al* 2004 MIRAGE: model description and evaluation of aerosols and trace gases *J. Geophys. Res.* **109** D20210
- Emmons L K *et al* 2010 Description and evaluation of the model for ozone and related chemical tracers, version 4 (MOZART-4) *Geosci. Model Dev.* **3** 43–67
- Engelhart G J, Asa-Awuku A, Nenes A and Pandis S N 2008 CCN activity and droplet growth kinetics of fresh and aged monoterpene secondary organic aerosol *Atmos. Chem. Phys.* **8** 3937–49
- Farina S C, Adams P J and Pandis S N 2010 Modeling global secondary organic aerosol formation and processing with the volatility basis set: implications for anthropogenic secondary organic aerosol *J. Geophys. Res.* **115** D09202
- Gettelman A, Liu X, Ghan S J, Morrison H, Park S and Conley A J 2010 Global simulations of ice nucleation and ice supersaturation with an improved cloud scheme in the community atmospheric model *J. Geophys. Res.* **115** D18216
- Ghan S J and Easter R C 2006 Impact of cloud-borne aerosol representation on aerosol direct and indirect effects *Atmos. Chem. Phys.* **6** 4163–74
- Ghan S J and Zaveri R A 2007 Parameterization of optical properties for hydrated internally mixed aerosol *J. Geophys. Res.* **112** D10201
- Goto D, Takemura T and Nakajima T 2008 Importance of global aerosol modeling including secondary organic aerosol formed from monoterpene *J. Geophys. Res.* **113** D07205
- Gunthe S S *et al* 2009 Cloud condensation nuclei in pristine tropical rainforest air of Amazonia: size-resolved measurements and modeling of atmospheric aerosol composition and CCN activity *Atmos. Chem. Phys. Discuss.* **9** 3811–70
- Hudson J G and Da X Y 1996 Volatility and size of cloud condensation nuclei *J. Geophys. Res.* **101** 4435–42
- Iacono M J, Delamere J, Mlawer E, Shephard M, Clough S and Collins W 2008 Radiative forcing by long-lived greenhouse gases: calculations with the AER radiative transfer models *J. Geophys. Res.* **113** D13103
- Intergovernmental panel on Climate Change (IPCC) 2007 *Climate Change 2007: The Physical Science Basis* (New York: Cambridge University Press)
- Jimenez J L *et al* 2009 Evolution of organic aerosols in the atmosphere *Science* **326** 1525–9
- Juranyi Z *et al* 2009 Influence of gas-to-particle partitioning on the hygroscopic and droplet activation behaviour of alpha-pinene secondary organic aerosol *Phys. Chem. Chem. Phys.* **11** 8091–7
- Kanakidou M *et al* 2005 Organic aerosol and global climate modelling: a review *Atmos. Chem. Phys.* **5** 1053–123
- King S M, Rosenoern T, Shilling J E, Chen Q and Martin S T 2007 Cloud condensation nucleus activity of secondary organic aerosol particles mixed with sulfate *Geophys. Res. Lett.* **34** L24806
- King S M, Rosenoern T, Shilling J E, Chen Q and Martin S T 2009 Increased cloud activation potential of secondary organic aerosol for atmospheric mass loadings *Atmos. Chem. Phys.* **9** 2959–71
- King S M, Rosenoern T, Shilling J E, Chen Q, Wang Z, Biskos G, McKinney K A, Poschl U and Martin S T 2010 Cloud droplet activation of mixed organic-sulfate particles produced by the photooxidation of isoprene *Atmos. Chem. Phys.* **10** 3953–64
- Köhler H 1936 The nucleus in and the growth of hygroscopic droplets *Trans. Faraday Soc.* **32** 1152–61
- Kroll J H, Ng N L, Murphy S M, Flagan R C and Seinfeld J H 2006 Secondary organic aerosol formation from isoprene photooxidation *Environ. Sci. Technol.* **40** 1869–77
- Lamarque J F *et al* 2010 Historical (1850–2000) gridded anthropogenic and biomass burning emissions of reactive gases and aerosols: methodology and application *Atmos. Chem. Phys.* **10** 7017–39
- Liu X, Penner J E and Herzog M 2005 Global simulation of aerosol dynamics: model description, evaluation, and interactions between sulfate and nonsulfate aerosols *J. Geophys. Res.* **110** D18206
- Liu X *et al* 2008 Indirect effect in NCAR CAM: sensitivity to aerosol-cloud parameterizations *Eos Trans. AGU* **89** (53) Fall Meet. Suppl., Abstract A32A-03
- Liu X *et al* 2010 Toward a minimal representation of aerosol direct and indirect effects *J. Clim.* submitted
- Lohmann U and Ferrachat S 2010 Impact of parametric uncertainties on the present-day climate and on the anthropogenic aerosol effect *Atmos. Chem. Phys. Discuss.* **10** 19195–217
- Lohmann U, Feichter J, Penner J and Leitch R 2000 Indirect effect of sulfate and carbonaceous aerosols: a mechanistic treatment *J. Geophys. Res.* **105** 12193–206

- Moffet R C and Prather K A 2009 *In situ* measurements of the mixing state and optical properties of soot with implications for radiative forcing estimates *Proc. Natl Acad. Sci. USA* **106** 11872–7
- Morrison H and Gettelman A 2008 A new two-moment bulk stratiform cloud microphysics scheme in the community atmosphere model, version 3 (CAM3). Part I: description and numerical tests *J. Clim.* **21** 3642–59
- Neale R B, Richter J H and Jochum M 2008 The impact of convection on ENSO: from a delayed oscillator to a series of events *J. Clim.* **21** 5904–24
- Neale R, B *et al* 2010 Description of the NCAR Community Atmosphere Model (CAM 5.0) *NCAR Technical Note* (available from: http://www.cesm.ucar.edu/models/cesm1.0/cam/docs/description/cam5_desc.pdf)
- Ng N L *et al* 2007 Effect of NO_x level on secondary organic aerosol (SOA) formation from the photooxidation of terpenes *Atmos. Chem. Phys.* **7** 5159–74
- Park S and Bretherton C S 2009 The University of Washington shallow convection and moist turbulence schemes and their impact on climate simulations with the community atmosphere model *J. Clim.* **22** 3449–69
- Park S *et al* 2010 Revised stratiform macrophysics in the Community Atmosphere Model *J. Clim.* in preparation
- Petters M D, Carrico C M, Kreidenweis S M, Prenni A J, DeMott P J, Collett J L and Moosmuller H 2009 Cloud condensation nucleation activity of biomass burning aerosol *J. Geophys. Res.* **114** D22205
- Petters M D and Kreidenweis S M 2007 A single parameter representation of hygroscopic growth and cloud condensation nucleus activity *Atmos. Chem. and Phys.* **7** 1961–71
- Posfai M, Simonics R, Li J, Hobbs P V and Buseck P R 2003 Individual aerosol particles from biomass burning in southern Africa: 1. Compositions and size distributions of carbonaceous particles *J. Geophys. Res.* **108** 8483–96
- Prenni A J, Petters M D, Kreidenweis S M, DeMott P J and Ziemann P J 2007 Cloud droplet activation of secondary organic aerosol *J. Geophys. Res.* **112** D10223
- Presto A A, Hartz K E H and Donahue N M 2005 Secondary organic aerosol production from terpene ozonolysis. 2. Effect of NO_x concentration *Environ. Sci. Technol.* **39** 7046–54
- Schulz M *et al* 2006 Radiative forcing by aerosols as derived from the AeroCom present-day and pre-industrial simulations *Atmos. Chem. Phys.* **6** 5225–46
- Twomey S 1977 Influence of pollution on shortwave albedo of clouds *J. Atmos. Sci.* **34** 1149–52
- Vestin A, Rissler J, Swietlicki E, Frank G P and Andreae M O 2007 Cloud-nucleating properties of Amazonian biomass burning aerosol: Cloud condensation nuclei measurements and modeling *J. Geophys. Res.* **112** D14201
- Wang J, Lee Y N, Daum P H, Jayne J and Alexander M L 2008 Effects of aerosol organics on cloud condensation nucleus (CCN) concentration and first indirect aerosol effect *Atmos. Chem. Phys.* **8** 6325–39
- Wang J, Cubison M J, Aiken A C, Jimenez J L and Collins D R 2010 The importance of aerosol mixing state and size-resolved composition on CCN concentration and the variation of the importance with atmospheric aging of aerosols *Atmos. Chem. Phys.* **10** 7267–83